THE ERS-1 SAR PERFORMANCE: A FINAL UPDATE

P.J. Meadows[(1)], H. Laur[(2)], B. Rosich[(2)] & B. Schättler[(3)]

(1) BAE SYSTEMS Advanced Technology Centres, West Hanningfield Road,
Great Baddow, Chelmsford, Essex, CM2 8HN, United Kingdom.
Email: peter.meadows@baesystems.com

(2) European Space Agency, Directorate of Application Programmes,
ESRIN, 00044 Frascati, Italy.

(3) German Aerospace Centre, German Remote Sensing Data Centre,
Algorithms and Processors, DLR Oberpfaffenhofen 82234 Wessling, Germany

ABSTRACT

The performance of the ERS-1 Synthetic Aperture Radar (SAR) was routinely assessed at the ESA Product and Archiving Facilities (PAFs) via a variety of quality assessment and calibration measures. This paper gives the final ERS-1 SAR quality assessment and radiometric calibration results including internal calibration, ADC power loss implications, stability, noise equivalent radar cross-section measurements and calibration of products processed with nominal replica pulses. Also given are expressions to calculate the radar cross-section of both distributed and point targets as well as ERS-1 attitude and SAR Doppler behaviour derived from SAR imagery.

1. INTRODUCTION

The ERS-1 SAR mission operated between July 1991 and March 2000. It, along with ERS-2 [1], fully lived up to its expectations by successfully demonstrating the ability of imaging radars to provide valuable long-term earth observation data to many categories of users.

Users required the SAR products from the ERS-1 SAR to be calibrated (absolutely or relatively). Absolute calibration supports the geophysical interpretation of SAR data by relating the digital values in data products to the physical and meaningful estimation of the normalised radar cross-section σ^o (also referred to as the backscattering coefficient). Relative calibration enables SAR products from either ERS-1 or ERS-2 to be compared with each other. The importance of using calibrated ERS SAR imagery has been demonstrated for the application of ocean wind speed extraction [2] and land applications [3, 4].

2. QUALITY ASSESSMENT

The quality of ERS-1 SAR imagery has been assessed via impulse response function (IRF) measurements using the three ESA transponders deployed in The Netherlands [5]. These measurements include the azimuth and range spatial resolutions, peak sidelobe ratio and integrated sidelobe ratio (see [2] for definitions). Table I gives values for these parameters from the PRI and SLCI products; as the PRI product range resolution varies across the swath, the table gives the range resolution converted to an incidence angle of 23°. The PRI results have been derived for measurements taken throughout the lifetime of ERS-1 while the SLCI results are derived from a set of 15 products acquired between January and March 1997. Figure 1(a) shows the PRI azimuth resolution as a function of acquisition date and Figure 1(b) shows the range resolution as a function of incidence angle for ERS-1 PRI products. The solid line and curve in these figures show the theoretical spatial resolutions. In addition, Figures 1(c) and 1(d) show the peak and integrated sidelobe ratios as a function of acquisition date for ERS-1 PRI products.

Table I and Figure 1 show that the measured azimuth and range resolutions compare well with theoretical values (20.76m for PRI azimuth resolution, 24.67m for PRI range resolution at 23° incidence angle, 4.82m for SLCI azimuth resolution and 9.64m for SLCI slant range resolution). The sidelobe ratios are all low and acceptable.

Parameter	PRI	SLCI
Azimuth resolution (m)	21.58±0.43m	5.32±0.02m
Range resolution	25.04±0.26m	9.66±0.06m
Peak sidelobe ratio	-15.9±0.8dB	-20.4±0.6dB
Integrated sidelobe ratio	-12.1±1.6dB	-14.8±1.2dB

Table I. ERS-1 SAR PRI and SLCI image quality parameters derived from the ESA transponders

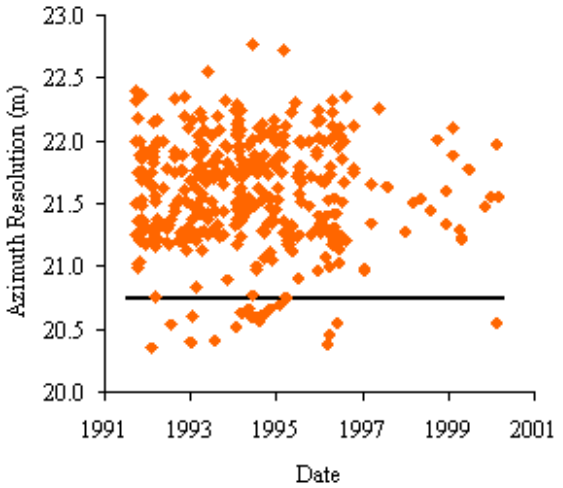

Figure 1(a). ERS-1.SAR.PRI azimuth resolution derived from the ESA transponders (the line is theoretical azimuth resolution)

The ESA transponders have also been used to derive the point target azimuth ambiguity ratio when the ambiguity background is sufficiently low to enable a measurement to be made (see [2] for further details). Based on the measurement of 13 ERS-1 SAR ambiguities in PRI products, the average azimuth ambiguity ratio is -27.8±3.1dB while the average difference in the measured and theoretical azimuth locations of the ambiguities is only 7.8±4.8m (i.e. less than one pixel). These results indicate an excellent ambiguity performance for the ERS-1 SAR.

Large uniform distributed targets can be used to estimate the image radiometric resolution. ERS-1 PRI and SLCI products give radiometric resolutions of 2.07dB and 3.03dB respectively. The theoretical values are 1.98dB for the PRI product and 3.01dB for the SLCI product.

Proceedings of the CEOS SAR Workshop, Tokyo, Japan, on 2-5 April 2001. NASDA publication EORC-061.

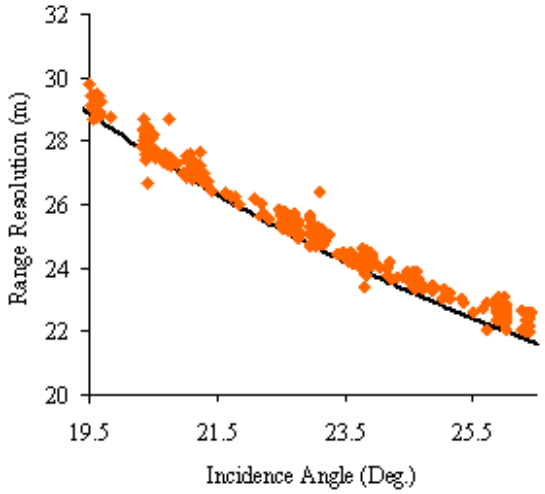

Figure 1(b). ERS-1.SAR.PRI range resolution derived from the ESA transponders (the curve is the theoretical range resolution)

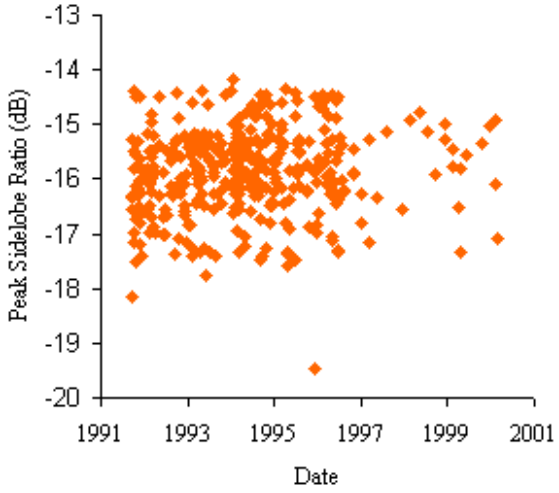

Figure 1(c). ERS-1.SAR.PRI peak sidelobe ratio derived from the ESA transponders

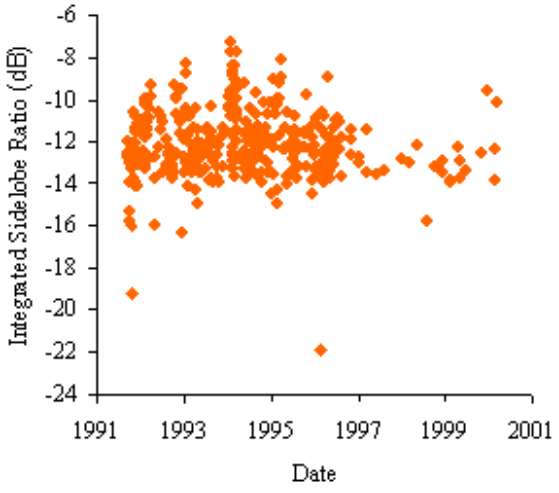

Figure 1(d). ERS-1.SAR.PRI integrated sidelobe ratios derived from the ESA transponders

One source of additional point targets for quality assessment is ERS SAR ground receiving stations [6]. As these are used to acquire ERS SAR raw data in real time, they will be pointing towards the satellite while acquiring the data. Image quality parameters have been derived for the ESA ground station at Kiruna, Sweden. Unfortunately this ground station has an extremely saturated IRF with an estimated radar cross-section of 71dBm^2 (cf. 57dBm^2 for the ESA transponders). However, the ground station azimuth ambiguities are sufficiently strong to enable some IRF parameters to be measured. These have a radar cross-section of approximately 47.5dBm^2 but very little sidelobe structure is visible. Table II gives the spatial resolution and sidelobe ratios; acceptable mean values are found but the sidelobe ratios are poor due to lack of sidelobes in the ambiguities. The main difference between the ground station quality parameters and those derived from the ESA transponders is that the standard deviation of the measurements is greater; this indicates that if a sufficient number of measurements are made, the ground station will give acceptable IRF values.

Parameter	Kiruna
Azimuth resolution	22.70±0.85m
Range resolution (at 23°)	26.30±0.93m
Peak sidelobe ratio	-7.8 ±1.2dB
Integrated sidelobe ratio	-4.3±0.9dB

Table II. ERS-1 SAR PRI image quality parameters derived from the Kiruna ground station.

3. RADIOMETRIC CALIBRATION

The radiometric calibration of ERS-1 SAR products is achieved via internal and external calibration to determine equations that can be used to calculate the radar cross-section of point and distributed targets (see sections 4 and 5). External calibration comprised elevation antenna pattern derivation using the Amazon rain forest [7] and the use of the ESA transponders for derivation of the image product calibration constants. The radiometric calibration corrections for ERS-2 ADC power loss are required to be carried out by the user.

3.1 Internal Calibration

The internal calibration of the ERS-1 SAR was assessed via calibration pulse, replica pulse and noise signal powers. The calibration pulse and noise signal are available at the start and end of each imaging sequence while the replica pulses are available throughout an imaging sequence. The calibration pulse measures the majority of any gain drift from image sequence to image sequence while the replica pulse monitors any gain drift during the imaging sequence when the more representative calibration pulse is not available. In fact, the power of the calibration pulse is the best guide we have for the transmitted pulse power. The SAR processors at the PAFs make no direct use of the calibration pulse power while the replica pulse is used for the range compression part of the processing.

Calibration pulse, replica pulse and noise signal powers from ERS-1 SAR data archived at the UK-PAF are shown in Figure 2. Note that ERS-1 was placed in standby mode in June 1996; after this date the amount of data acquired reduced significantly. For the period up to early 1998, the calibration pulse power was, for the most part, stable. The replica pulse power, during the same period showed variation of up to 2dB. It has been concluded that the ERS-1 SAR calibration pulse power (and hence the transmitter pulse power) is independent of the replica pulse power (see Figure 2(c)). This is of particular importance for ERS-1 SAR image calibration as the image variations introduced by the range compression part of the processing (which uses a replica pulse) need to be removed. This is achieved via a replica pulse correction in the expression used for the calculation of radar cross-

section which relates the image replica power to the replica power of the reference image used to derive the calibration constant K (see sections 4 and 5).

During the period from early 1998, the calibration pulse power was consistently high compared to before this date. This change indicates that the transmitter pulse power increased shortly after a 38% reduction in available power from the ERS-1 solar panels that occurred on 29 December 1997 [8]. A consequence of the change in transmitter pulse power was that the ERS-1 SAR calibration constant needed to be revised for data acquired from early 1998. Using ERS-1 SAR transponder measurements from 24 February 1998, a revised calibration constant was measured to be 0.79dB higher than previously. Thus, for example, ERS-1 VMP PRI products processed at the UK-PAF have a revised calibration constant of 59.03dB (799000) cf. 58.24dB (666110) previously while for the SLCI products, the revised K is 48.92dB (78000) cf. 48.13dB (65026). The decrease in replica pulse power (Figure 2(b)) for the same period is compensated for by the ERS-1 SAR replica pulse power correction. Note that the ERS-1 noise signal power remained constant throughout its lifetime.

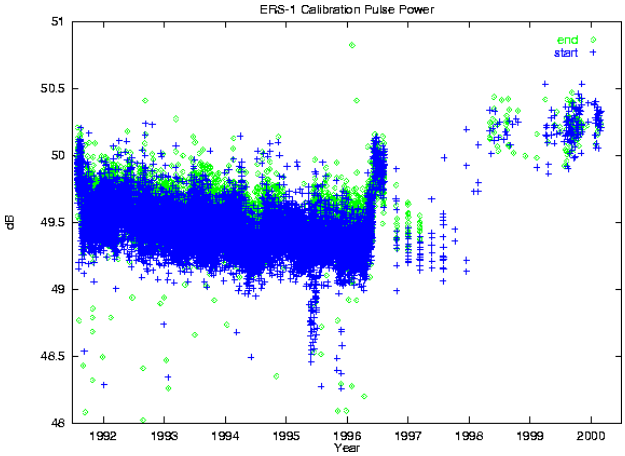

Figure 2(a). ERS-1 SAR Calibration Pulse Powers

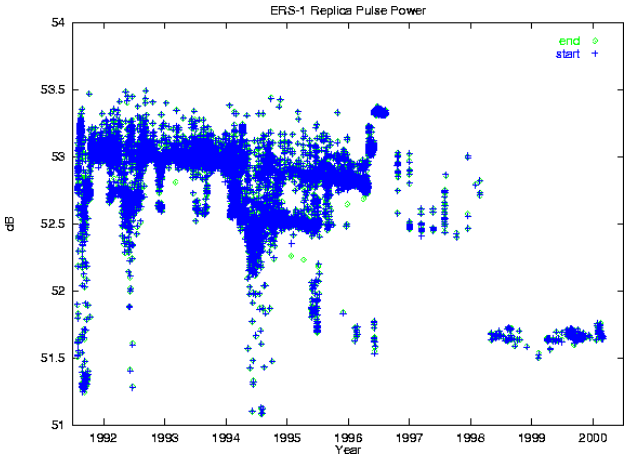

Figure 2(b). ERS-1 SAR Replica Pulse Powers

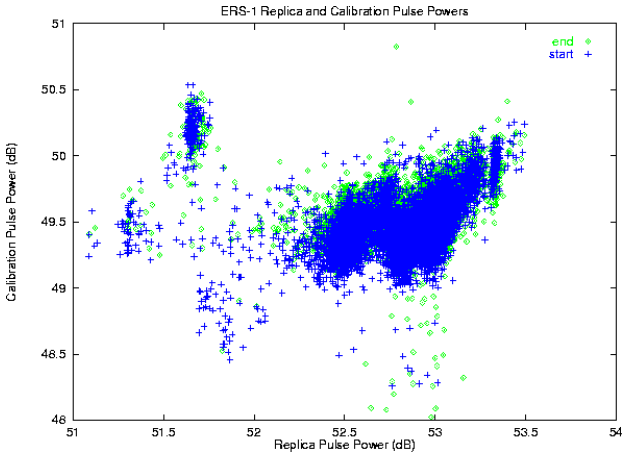

Figure 2(c). Relationship between ERS-1 Replica and Calibration Pulse Powers

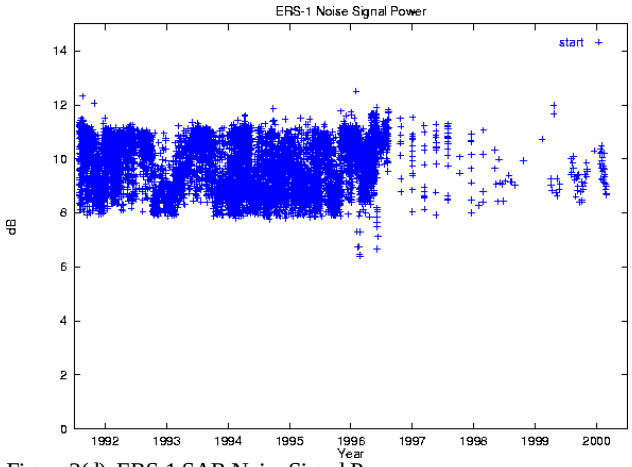

Figure 2(d). ERS-1 SAR Noise Signal Powers

3.2 ADC Power Loss Correction

ERS SAR raw data are quanitsed to 5 bits within the on-board Analogue to Digital Convertor (ADC). The distribution of the I and Q channels is Gaussian and so if the input signal is high, a large number of data values will occupy the lowest and highest quantisation levels, i.e. saturation will occur. Any saturation will lead to the situation where the output power from the ADC will be less than the input power (i.e. there is a power loss). The gain of the ERS-1 SAR was such that a significant proportion of imagery was affected by saturation [9]. For example, Figure 3(a) shows an ERS-1.SAR.PRI image of Zeeland, The Netherlands (Orbit 13946, Frame 1035, 16 March 1994) together with a selection of raw data histograms. The vertical scale of each histogram is the same to enable the relative distribution of raw data to be shown. Ideally, the distribution of raw data samples should be a Gaussian falling to close to zero at the upper and lower quantisation levels. This is clearly not the case.

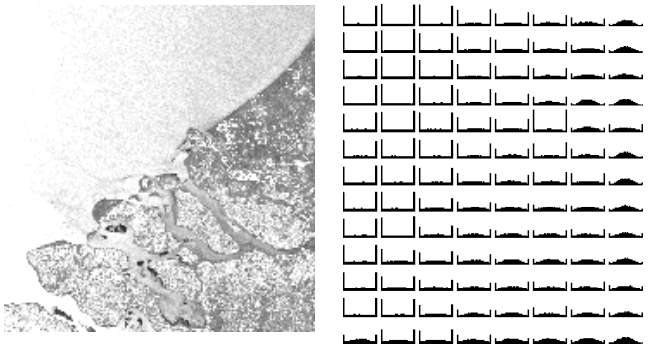

Figure 3(a). ERS-1 PRI image and raw data histograms of Zeeland, The Netherlands

A method was developed [9, 10] whereby the ADC power loss correction could be estimated directly from PRI image products. This was achieved by the removal of various functions from the PRI image and the use of a look-up table. The various functions are the elevation antenna pattern, range spreading loss and the replica pulse correction. This method is ideal for large homogeneous regions, such as the oceans or Greenland, and is adequate for other types of distributed targets. It is estimated that the ADC power loss can be calculated to better than 0.5dB for distributed targets [9]. The method does have limitations where there are a large number of bright point targets within the SAR footprint (approximately 5km in azimuth and 15km in ground range) such as is the case for large towns and cities. For such regions, the method underestimates the ADC power loss by up to 1 dB [3].

One consequence of the large instantaneous footprint of the ERS-1 SAR (approximately 5km in azimuth and 15km in ground range) is that land regions adjacent to high radar cross-section regions, such as the oceans under strong wind conditions, can also have high ADC power losses. Figure 3(b) shows a contour plot of the ADC power loss (left) and radar cross-section (right) derived from Zeeland PRI product shown in Figure 3(a) where the adjacent North Sea has a high backscatter. There is a high concentration of ADC power loss contours along the coastal region indicating a change in power loss in this region. This change is not just restricted to the ocean but also to the neighboring coastal region. The ESA transponders were deployed at three locations across this scene during the ERS-1 3-day repeat period ice mission phases. The ADC power loss of each transponder was affected by the state of the adjacent ocean, with the transponders nearest to the coast being affected more. This effect also occurred when the transponders were moved to Flevoland as the Ijsselmeer and Marker Meer open water regions were nearby.

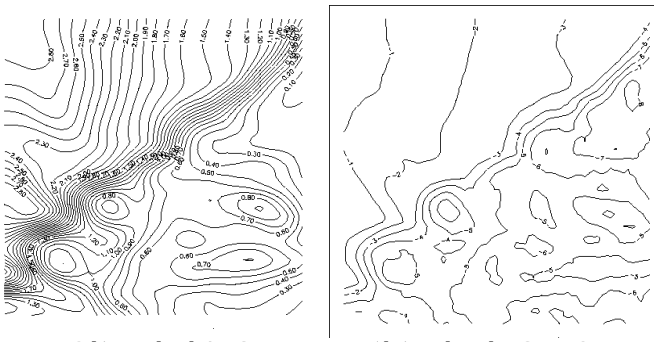

Figure 3(b). Zeeland ADC Power Loss (dB) and Radar Cross-Section (dB)

A good demonstration of the need to include the ADC power loss when deriving radar cross-sections from ERS-1 SAR imagery is the application of ocean wind speed extraction. This is because the radar cross-section over the oceans can be very high and occurs over very large regions hence leading to large ADC power losses. For this application, comparison of radar cross-section range profiles with a wind retrieval model is made. The model generally used is the C-band wind scatterometer model CMOD4 which gives the ocean radar cross-section as a function of wind speed, wind direction and incidence angle [11]. Figure 4 shows the CMOD4 model for wind speeds between 2 m/s and 26 m/s in the downwind direction (i.e. wind blowing away from the radar). The upwind curves are similar to those for downwind while the crosswind curves are several dB smaller. Also shown in Figure 4 are the ERS-1 SAR derived wind speed when no ADC power loss correction is used in the calibration. The shapes of these curves are a function of those parameters which affect the raw data power such as the elevation antenna pattern. Figure 4 shows that for a CMOD4 wind speed of 26 m/s and at near range, ERS-1 SAR imagery, without the ADC power loss correction, will determine a wind speed of only approximately 6 m/s. Thus the ERS-1 derived wind speed is significantly lower than the CMOD4 wind speed.

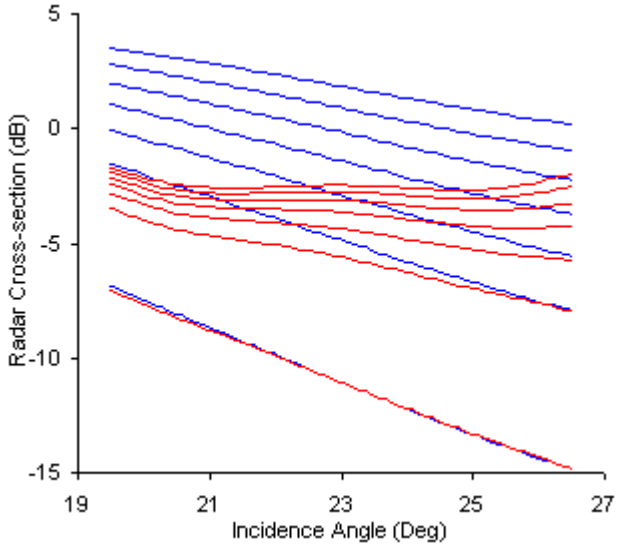

Figure 4. The CMOD4 radar cross-section model (blue curves) for downwind wind direction and the ERS-1 derived radar cross-sections (red curves) if no ADC power loss correction were applied (for wind speeds between 2 m/s (bottom) and 26 m/s (top) and steps of 4 m/s).

3.3 Stability

The stability the ERS-1 SAR instrument is important for calibration. This has been measured throughout the lifetime of the instrument using the three ESA transponders deployed in Flevoland and Zeeland in the Netherlands. In particular, the measured radar cross-sections of the transponders have been compared to their actual radar cross-section values. This relative transponder radar cross-section (after all calibration corrections have been applied) has been routinely calculated as is shown in Figure 5.

The measured mean radiometric results for the ERS-1 SAR using the ESA transponders is shown in Table III (based on measurements between September 1991 and February 2000). The radiometric stability is defined as the standard deviation of the transponder radar cross-section measurements, the radiometric accuracy is the mean difference between the actual and measured transponder radar cross-sections and the peak to peak radar cross-section gives the maximum difference in transponder radar cross-section measurements.

These results together with internal calibration measurements indicate an excellent stability while the radiometric accuracy is very good and the peak to peak values is acceptable (given the quoted accuracy of the calibration constant K is ±0.4 dB). There has also been no degradation in the performance of the ERS-1 SAR with time and hence no reduction in the accuracy with which the image products can be calibrated.

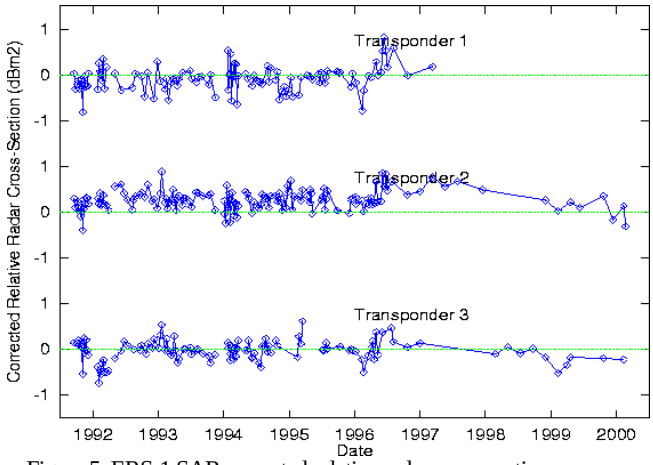

Figure 5. ERS-1 SAR corrected relative radar cross-section.

Parameter	
Radiometric stability	0.24dB
Radiometric accuracy	0.05dB
Peak to peak radar cross-section	1.42dB

Table III. ERS-1 SAR radiometric results derived from the ESA transponders

The measured radar cross-section of the Kiruna ground station azimuth ambiguities have also been used to derive the stability of the ERS-1 SAR by using the average of two ambiguities in each scene. The use of the azimuth ambiguities assumes that the ERS SAR azimuth antenna pattern is stable. Figures 6(a) and 6(b) show the ERS-2 Kiruna ambiguity radar cross-section relative to the mean value as a function of date and incidence angle. Figure 6(b) also shows that there is no obvious radar cross-section trend with incidence angle. Table IV gives the mean radar cross-section, stability and peak to peak radar cross-section values of the Kiruna ambiguities. These results are higher than the transponder results given in Table III.

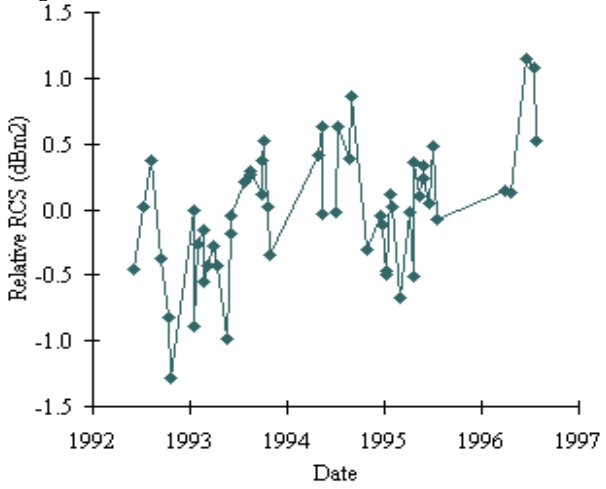

Figure 6(a). Kiruna azimuth ambiguity relative radar cross-section as a function of date

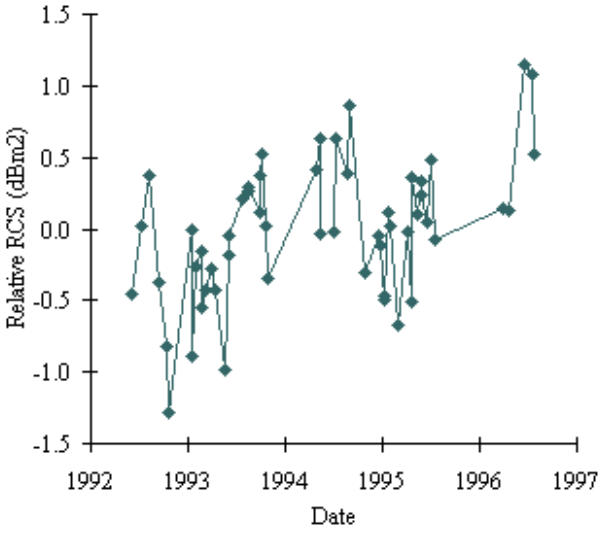

Figure 6(b). Kiruna azimuth ambiguity relative radar cross-section as a function of incidence angle

Parameter	
Radar cross-section	47.23dBm^2
Radiometric stability	0.49dB
Peak to peak RCS	2.43dB

Table IV. ERS-1 SAR radiometric results derived from the Kiruna ground station

3.4 Noise Equivalent σ^o

The upper limit to the noise equivalent σ^o (NEσ^o) of an image can be estimated by measuring the radar cross-section of low intensity regions (usually oceans). A small number of ERS-1 SAR PRI products with suitable regions present give an estimated NEσ^o of -26.2dB. Assuming that the noise is thermal in origin, then the NEσ^o is expected to change across the swath for PRI products due to the application of the elevation antenna pattern. It has been possible to select an ERS-1.SAR.PRI product with a low backscatter region extending from near to far range (Orbit 14691, Frame 1197, 7 May 1994). Figure. 7 shows the low intensity region σ^o measurements for a 6km azimuth strip stretching from near to far range together with the ERS-1 SAR elevation antenna pattern. It can be seen that the elevation pattern and the σ^o profile fit very well indicating that the noise is indeed thermal in origin.

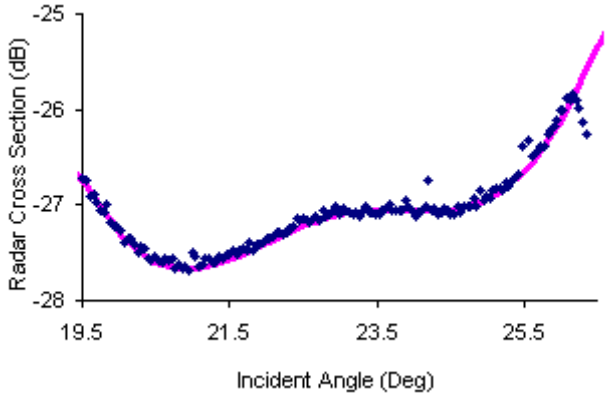

Figure 7. ERS-1.SAR.PRI Noise Equivalent σ^o for an ERS-1.SAR.PRI product (Orbit 14691, Frame 1197, 7 May 1994)

3.5 Nominal Replica Pulse Products

A small number of processed using the ESA Processing and Archiving Facility SAR Verification Mode Processor (VMP) have been generated using a nominal replica pulse rather than a replica generated at the time of imaging (an extracted replica). Products generated with a nominal replica have significantly higher pixel values than products generated using an extracted replica. ERS-1 SAR products are corrected by reducing the image intensity by factor of 291.52 (24.65dB).

4. DISTRIBUTED TARGET RADAR CROSS-SECTION DERIVATION

The expression required to calculate the radar cross-section of a distributed target from ERS-1.SAR.PRI imagery is:-

$$\sigma^o = \frac{<A^2>}{K} \frac{\mathrm{Sin}\alpha_D}{\mathrm{Sin}\alpha_{Ref}} \frac{\mathrm{Image\,Replica\,Power}}{\mathrm{Reference\,Replica\,Power}} \mathrm{Power\,Loss} \qquad (1)$$

where:-

σ^o = distributed target radar cross-section,

$<A^2>$ = average pixel intensity of a distributed target,

A = pixel digital number,

K = PRI calibration constant,

α_D = distributed target incidence angle (including any local surface slope),

α_{Ref} = reference incidence angle (23°),

Image Replica Power = power of replica pulse used to process the image,

Reference Replica Power = replica pulse power of the ERS-1 SAR reference image (205229),

Power Loss = ADC power loss.

The expressions required to calculate the radar cross-section of a distributed target from detected complex data are different from the PRI products. This is because no elevation antenna pattern correction and range spreading loss have been applied to the SLCI products. For detected ERS-1.SAR.SLCI products the required expression is:-

$$\sigma^o = \frac{<A^2>}{K} \frac{\mathrm{Sin}\alpha_D}{\mathrm{Sin}\alpha_{Ref}} \frac{\mathrm{Image\,Replica\,Power}}{\mathrm{Reference\,Replica\,Power}} \mathrm{Power\,Loss} \frac{1}{G(\theta_D)^2} \frac{R_D^3}{R_{Ref}^3} \qquad (2)$$

where in addition to the terms used for PRI distributed target radar cross-section derivation:-

K = SLCI calibration constant,

$G(\theta_D)^2$= elevation antenna pattern gain at the distributed target,

θ_D = distributed target look angle,

R_D = distributed target slant range,

R_{Ref} = reference slant range (847.0 km).

The replica pulse power correction is exactly the same as for PRI products while the method for calculating the ADC power loss considers the fact that detected SLCI imagery is in slant range and has no elevation antenna pattern or range spreading loss applied.

Specific details of how to calculate the radar cross-section of distributed targets (including the replica pulse and ADC power loss) for ERS-1 SAR PRI and SLCI products can be found in [10].

5. POINT TARGET RADAR CROSS-SECTION DERIVATION

The expression required to calculate the radar cross-section of a point target from ERS-1.SAR.PRI imagery is:-

$$\sigma = \frac{I_P}{C_F} \frac{P_A}{K} \frac{\mathrm{Sin}\alpha_P}{\mathrm{Sin}\alpha_{Ref}} \frac{\mathrm{Image\,Replica\,Power}}{\mathrm{Reference\,Replica\,Power}} \mathrm{Power\,Loss} \qquad (3)$$

where in addition to the terms used for distributed targets:-

σ = point target radar cross-section,

I_P = total power in the point target mainlobe,

C_F = relative power in the point target sidelobes = 1/(1+ISLR),

ISLR = integrated sidelobe ratio,

P_A = PRI product pixel area (156.25m^2),

α_P = point target incidence angle.

For point target derivation from ERS-1.SAR.SLCI products requires that the data is resampled to preserve all the statistical properties of the data. This is needed to ensure that the detected image is adequately sampled (i.e. at twice per resolution cell). As the ERS SAR complex data is sampled at once per resolution cell, a resampling factor of two is required. It is also necessary to ensure that the complex data power spectra is completely within the sampling window. If the power spectra is 'folded over' from one end of the sampling window to the other, then a spectrum shift is required. In the case where only the mean intensity of a distributed target is required (such as for the radar cross-section calculation) then it is possible to detect the complex data without resampling.

For detected ERS-1.SAR.SLCI products the required expression is:-

$$\sigma = \frac{I_P}{C_F} \frac{P_A}{K} \frac{1}{\mathrm{Sin}\alpha_{Ref}} \frac{1}{S_F^2} \frac{\mathrm{Image\,Replica\,Power}}{\mathrm{Reference\,Replica\,Power}} \mathrm{Power\,Loss} \frac{1}{G(\theta_P)^2} \frac{R_P^3}{R_{Ref}^3} \qquad (4)$$

where in addition to the terms used for PRI point target radar cross-section derivation:-

P_A = SLCI product pixel area (~30.8m^2),

K = SLCI calibration constant,

S_F = sampling factor for detection of SLCI data,

$G(\theta_P)^2$ = elevation antenna pattern gain at the point target,

θ_P = point target look angle,

R_P = point target slant range.

The derivation of the replica pulse and ADC power loss corrections are the same as for distributed targets.

6. ATTITUDE AND DOPPLER VARIATIONS

The piloting of the ERS-1 satellite throughout its lifetime was performed using three gyroscope (ERS-2 has operated using three, one and no gyroscopes [12]). UK-PAF SAR products have been used to monitor the satellite attitude (yaw and pitch [13]), the Doppler centroid frequency and the PRI product azimuth image extent for the portion of ERS-1 orbits where imagery is acquired by the ESA ground station at Kiruna, Sweden. Figure 8 shows the ERS-1 yaw, pitch, Doppler centroid frequency and azimuth image extent during the majority of its lifetime (using information from products used for routine analysis). It can be seen that there were several occasions, for imagery archived at the UK-PAF, when there was a larger than expected change in attitude and Doppler centroid frequency. This was due, primarily, to imagery

acquired during orbit maneouvres (imagery acquired during a maneouvre can still be processed but it may be unsuitable for interferometry). The negative Doppler Centroid frequencies are from ascending pass imagery while positive values are from descending pass imagery. Note that during the periods of abnormal attitude behaviour, the azimuth image extent of PRI products (Figure 8(d)) reduces from the nominal length of around 8200 pixels.

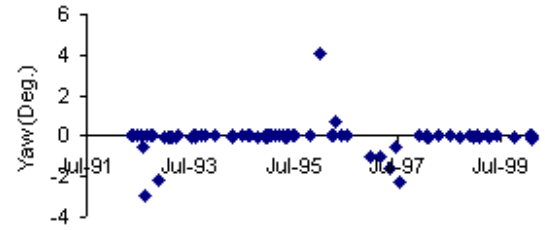

Figure. 8(a). ERS-1 Yaw

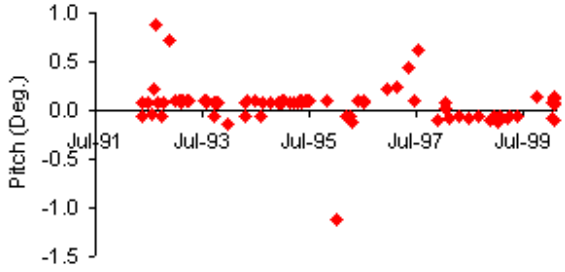

Figure. 8(b). ERS-1 Pitch

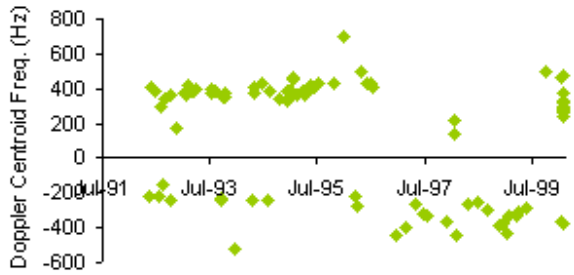

Figure. 8(c). ERS-1 Doppler Centroid Frequency

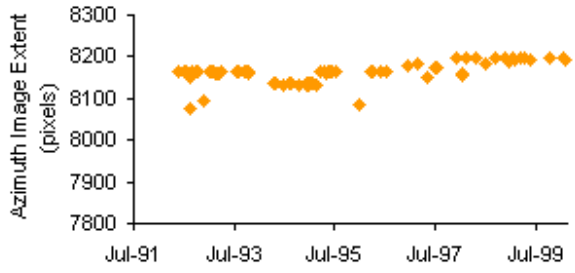

Figure. 8(d). ERS-1 PRI Azimuth Image Extent

7. CONCLUSIONS

This paper has given details of the performance of the ERS-1 SAR by consideration of quality assessment and radiometric calibration using the ESA transponder and the ERS ground receiving station at Kiruna together with other aspect of the ERS-1 SAR and its products. Results presented show that, during it lifetime, the ERS-1 SAR worked well with excellent quality assessment and radiometric calibration results.

8. ACKNOWLEDGEMENTS

The ERS SAR data used in this paper was processed at one of the ESA ERS Processing and Archiving Facilities. We would like to thank the staff at the UK-PAF for their support in the processing of this SAR data.

9. REFERENCES

[1] Meadows, P.J. & Rosich, B., 'The ERS-2 SAR Performance: a Further Update', These proceedings.

[2] Meadows, P.J., Laur, H., Sánchez, J.I. & Schättler, B., 'The ERS SAR Performances', Proceedings of the CEOS SAR Workshop, 3-6 February 1998, ESTEC, Noordwijk, The Netherlands, ESA WPP-138, 223-232.

[3] Meadows, P.J., Laur, H. & Schättler, B., 'The Calibration of ERS SAR Imagery for Land Applications', Proceedings of the 2nd International Workshop on Retrieval of Bio- & Geo-physical Parameters from SAR Data for Land Applications, 21-23 October 1998, ESTEC, Noordwijk, The Netherlands, ESA SP-441, 35-42.

[4] Meadows P.J., Laur, H. & Schättler, B., 'The Calibration of ERS SAR Imagery for Land Applications', Earth Observation Quarterly, No 62, June 1999.

[5] Woode, A.D., Desnos, Y-L. & Jackson, H., 'The Development and First Results from the ESTEC ERS-1 Active Radar Calibration Unit', IEEE Trans. Geosci. Remote Sensing, 30, 1122-1129, 1992.

[6] Meadows, P.J., 'The Use of Ground Receiving Stations for ERS SAR Quality Assessment', Proceedings of the CEOS SAR Workshop, 26-29 October 1999, Toulouse, France. ESA publication SP-450, 525-530.

[7] Laycock, J.E. & Laur, H., 'ERS-1 SAR Antenna Pattern Estimation', ESA/ESRIN, ES-TN-DPE-OM-JL01, Issue 1, Rev. 1, September 1994.

[8] Earth Observation Programme Board, 'ERS Mission Status following partial ERS-1 Solar Array Failure', ESA Information Note ESA/PB-EO/DOSTAG(98)3, April 1998.

[9] Meadows, P.J. & Wright, P.A., 'ERS-1 SAR Analogue to Digital Convertor Saturation', Proceedings of the CEOS SAR Workshop, Ann Arbour, 28-30 September 1994.

[10] Laur, H., Bally, P., Meadows, P., Sánchez, J., Schättler, B., Lopinto, E. & Esteban, D., 'ERS SAR Calibration: Derivation of the Backscattering Coefficient σ^o in ESA ERS SAR PRI Products', ESA/ESRIN, ES-TN-RS-PM-HL09, Issue 2, Rev. 5b, September 1998 (available via http://earth1.esrin.esa.it/ESC2).

[11] Stoffelen, A. & Anderton, D.L.T., 'ERS-1 Scatterometer Data Characteristics and Wind Retrieval Skill', Proceedings of the First ERS-1 Symposium - Space at the Service of our Environment, Cannes, 4-6 November 1992, ESA SP-359.

[12] Rosich, B., Meadows, P.J., Schättler, B., Grion. M. & Emiliani, G., 'The ERS-2 mono-gyro and extra backup piloting modes: impact on SAR performance', These proceedings.

[13] Esteban Fernández, D., Meadows, P.J., Schättler, B. & Mancini, P., 'ERS attitude errors and its impact on the processing of SAR data', Proceedings of the CEOS SAR Workshop, 26-29 October 1999, Toulouse, France. ESA publication SP-450, 597-605.